Siting and Segregation Effects of Simple Molecules in Zeolites MFI, MOR, and BOG

Louis A. Clark, Amit Gupta, and Randall Q. Snurr*

Department of Chemical Engineering and Center for Catalysis and Surface Science, Northwestern University Evanston, Illinois 60208

Received: February 17, 1998

The effect of the spatially heterogeneous nature of zeolite pores on molecular arrangement and adsorption is investigated. Three zeolites (MFI, MOR, and BOG) are chosen to represent structures containing dissimilar pore shapes and sizes. Four simple adsorbates (argon, methane, CF_4, and SF_6) are chosen as probes of varying size and interaction energy. Direct Monte Carlo integration of the partition function is used to determine free energies, potential energies and entropies of adsorption in spatially distinct regions of the zeolites at low loadings. These calculations lead to intuitive explanations of siting seen in one- and two-component grand canonical Monte Carlo simulations of adsorption. Both simulation techniques are implemented using the same potential model in identical zeolites. Owing to the similar nature of the two MFI channels, only small differences in adsorption free energies between channels are seen and segregation effects are minimal. Conversely, the very heterogeneous nature of MOR leads to substantial free energies differences and pronounced segregation. Confinement effects in the MOR side pockets produce a large entropic penalty for adsorption. The dissimilar 10-ring and 12-ring channels in BOG also lead to substantial segregation under many conditions. The siting distributions for the single-component systems are explained using filling and packing effects. The binary data is explained by introducing four qualitative models that can be used to classify the observed segregation.

Introduction

The wide assortment of known microporous crystalline structures provides an enormous range of properties that encourage their use in numerous applications. Some emerging applications include thin film sensors,[1] radioactive materials storage,[2] membrane separations,[3] and as hosts for chiral catalysts.[4] More established areas include adsorption separations and catalysis. Most of these applications, especially the more established ones, depend on the geometrical and chemical properties of the structure. For example, in adsorption separations zeolites are used to selectively adsorb one component of a mixture. It is the size, shape, and chemical properties of the zeolite pores that determine the selectivity, and therefore the practicality, of the separation.

Unfortunately, the direct relationship between pore structure and applications property is frequently missing. The difficulty of obtaining information about processes that occur on such a small scale and in such a heterogeneous environment has left many questions unanswered. These unknowns make design of microporous materials for desired applications difficult. In an ideal design situation, one would define the process and then choose a zeolite or other microporous material based solely on its known properties and their predicted effect on the process. In reality, one makes judgments based on educated guesses and experience and then refines the choice by experiment. Increased understanding of structure−property relationships will improve the efficiency of this design process. It is also likely to expand the use of the materials, as greater understanding gives rise to new ideas.

This paper concerns the effect of the pore geometry on the spatial distribution of adsorbed molecules within a zeolite structure. Knowledge of where the molecules adsorb is the most basic starting point for any fundamental description of adsorption. Single-component systems in heterogeneous adsorbents may display preferential siting in particular regions of the zeolite, and multicomponent systems may show preferential adsorption of dissimilar species into different regions as well. This separation of dissimilar species is called segregation. Dunne et al.[5] have recently stated that deviations from ideal adsorbed solution (IAS) theory stem from segregation in the adsorbed phase. Karavias and Myers provide support for this idea.[6] The interest in studying segregation stems from both understanding how the phenomenon might be useful in applications and understanding fundamentally why the structure produces segregation.

Zeolite catalysis provides a good example of how segregation effects could be put to use. Zeolites often possess distinctly different types of regions within the same structure. These different regions, characterized by their shape and average energy that a molecule feels within them, may contain higher proportions of a given adsorbed species. This segregation, coupled with other properties of the regions, may affect the catalytic selectivity, e.g., if some regions contain active sites that other regions lack.

Understanding the fundamentals of segregation is also important in adsorption separations. A separations material must be chosen to selectively adsorb one species while the external mixture, poor in the strongly adsorbed species, is drawn off. The desired selectivity is created by picking a zeolite such that the component to be removed has a significantly lower free energy of adsorption than the other components. The free energy difference can be obtained by picking a zeolite with a pore shape that "fits" the desired adsorbate well. It is differences in this "fit" that also cause molecules inside a zeolite to

* To whom correspondence should be addressed.

S1089-5647(98)01179-1 CCC: $15.00
Published on Web 08/06/1998

segregate. Chemical properties, such as the presence of functional groups, can also be quite significant but will not be considered here so as to focus attention on the geometric properties of the zeolite pore.

Segregation is difficult to study by direct experiment. It seems that, to date, only NMR techniques have been used to measure segregation. Xu et al.[7] attempted to measure the relative populations of argon and methane in the regions of mordenite (MOR) by analyzing T_1 proton relaxation times. They varied temperature and adsorbed phase composition and were able to make qualitative conclusions after assuming a model for the relaxation time. It may also be possible to exploit the chemical shift differences of highly polarizable molecules in different zeolite regions to measure segregation. For single-component measurements, Ripmeester noted ^{129}Xe chemical shift differences in the side pockets of MOR versus the 12-ring channels.[8] However, the presence of other sorbates also influences the chemical shift of the probes, which may make siting distinction via chemical shift difficult in mixtures.

Although no simulation work has explicitly focused on molecular segregation, selectivity during adsorption of binary mixtures has been studied.[9−19] Keffer et al.[18] briefly review their simulation work and that of others in idealized nanopores. They find that, at low loadings, sorbate−zeolite energetics are most important in determining the selectivity. At higher loadings, the individual abilities of the species to pack into the pores become significant. In both cases, the adsorbed phase composition is determined by minimizing the total free energy. The difference lies in whether interaction with the absorbent or with other adsorbates determines the selectivity. Van Tassel et al.[13] observe interesting selectivity effects in their grand canonical Monte Carlo (GCMC) simulations. They note a reversal in selectivity, favoring the normally weakly adsorbed species, at very high chemical potentials and attribute it to packing effects. In addition, they separate the roles of potential energy and entropy, greatly clarifying matters.

This paper considers adsorption of argon, methane, CF_4, and SF_6 mixtures in the zeolites silicalite (MFI), mordenite (MOR), and boggsite (BOG). Using the GCMC technique and Metropolis Monte Carlo integration of the configurational partition function, we are able to quickly predict and explain segregation effects in these systems. The sorbates were chosen for their varying size. In addition, methane, CF_4, and SF_6 represent likely candidates for NMR experiments. The paper first defines the potential model that we use and then explains how the regions themselves are defined. The definitions are followed by a complete description of the free energy calculations and a brief description of the GCMC calculations, which have been well treated previously. The remainder of the paper describes and explains first the single and then the binary component results on the basis of both enthalpic and entropic effects. Additional concepts and models will be introduced to rationalize the effects that predominate at higher loadings and in binary systems.

Potential Model

Argon, methane, CF_4, and SF_6 are modeled as simple Lennard-Jones spheres. All zeolites are studied in the siliceous, cation-free form. Zeolite−adsorbate interactions are modeled using pairwise interactions between only the zeolite oxygen atoms and the adsorbate. This approximation is justified by noting that the zeolite T-atoms are well shielded by the oxygens.[23] The zeolite itself is considered to be immobile; interatomic potentials for it are unneeded. Table 1 gives the adsorbate−adsorbate and the adsorbate-oxygen interaction parameters. Interaction parameters between dissimilar adsorbates were obtained using Lorentz−Berthelot mixing rules. Note that the size of adsorbates (σ) increases in the order argon, methane, CF_4, SF_6. All three zeolites, MFI, MOR, and BOG, are modeled using the same adsorbate-oxygen parameters.

TABLE 1: Potential Parameters Used in the Simulations[a]

interaction pair	ϵ/k (K)	σ (Å)	ref
Ar−Ar	124.07	3.42	20
Ar−oxygen	95.61	3.17	fit@77 K
CH_4−CH_4	148.00	3.73	28
CH_4−oxygen	133.33	3.21	28
CF_4−CF_4	134.04	4.66	17
CF_4−oxygen	109.60	3.73	17
SF_6−SF_6	222.10	5.13	21
SF_6−oxygen	147.21	3.97	26

[a] The sizes of the molecules can be inferred from the sorbate−sorbate value of σ.

The methane and CF_4 parameters have been experimentally validated in siliceous MFI (silicalite).[17] They reproduce single-component isotherms in siliceous MFI well at low loadings and to within 1 molecule/unit cell at high loadings. Heats of adsorption are reproduced to within 2 kJ/mol across the range of loadings. The same potentials were used in a molecular dynamics study of methane and CF_4 in silicalite. Diffusivities from these simulations matched those obtained from pulsed field gradient NMR studies well.[24] Smit et al.[25] compared various methane−silicalite potentials and found that the ones used here reproduced experimental results best.

Site Determination

To talk about segregation in microporous media, one must first divide the accessible pore space into subspaces. We call these subspaces *sites*, not to be confused with active sites. The pore space for an arbitrary zeolite can be intuitively divided into sites by taking the bounding surfaces to be the set of points at which trajectories near 0 K are equally likely to descend to energy minima at either side of the surface.[26,27] Physically, if one places a molecule into an arbitrary accessible position in a zeolite and then cools it to 0 K, it will move down its potential energy gradient into a minimum. The positions of the minima can thus be used to label all the accessible positions in a zeolite. Sites can be defined in other ways, too. For example, Goodbody et al.[28] used geometric, rather than energetic, means to define sites in MFI. The method used here is general and natural since it results in sites that are separated by energy barriers.

Our algorithm for finding sites was implemented as follows.[26,27] First, all unique minima of the potential energy hypersurface are identified using the BFGS algorithm[29] from a large number of randomly generated coordinates. The minima are then tabulated and visualized. Once visualized they can be grouped into sets corresponding to the natural topology of the zeolite. For example, all the potential minima inside the MFI zigzag channel can be labeled as belonging to one *site*. The accessible pore volume is then approximated as a collection of cubelets. We typically use a grid spacing of ca. 0.2 Å because it provides a good compromise between numerical accuracy and storage space constraints. The next step consists of placing a molecule in each cubelet, calculating its potential energy gradient vector, and then stepping down the vector until the molecule has moved into one of the pretabulated minima. The cubelet is then given the same site label as the minimum. The result is a classification of the accessible space into regions that are reasonable both from an energetic and an intuitive viewpoint.

Free Energy Calculations

The free energies for molecules confined in the various sites were determined by direct evaluation of the configurational partition function. The complete expression for the semiclassical canonical partition function is the product of a kinetic energy term and a configurational term.[30]

$$Q(NVT) = \frac{1}{N!}\left(\frac{2\pi mkT}{h^2}\right)^{(3N)/2} Z_N \tag{1}$$

$$Z_N = \int_V \exp\left(\frac{-V}{kT}\right) \mathrm{d}\vec{r}_1 ... \mathrm{d}\vec{r}_N \tag{2}$$

Here $Q(NVT)$ is the canonical partition function and Z_N is the configurational part of the partition function. N is the number of indistinguishable, monatomic species in the integration volume V. The integration volume is composed of all sites of a given type within a single unit cell. For example, the integration volume for the intersections in silicalite is the combined volume of four separate intersection sites. V is the potential energy of the system, and the integration is over the $3N$ coordinates of the molecules in the system. m, T, k, h are the mass per molecule, system temperature, Boltzmann's constant, and Planck's constant, respectively. It is possible to avoid calculating the kinetic energy term if one picks a reference state such that it is constant between the two states. One state is the adsorbed molecules, and the other is an ideal gas reference state. The canonical ensemble expression for the Helmholtz energy can then be applied.

$$\Delta A = A - A^{\mathrm{ref}} = -kT \ln\left(\frac{Q}{Q^{\mathrm{ref}}}\right) = -kT \ln\left(\frac{Z_N}{Z_N^{\mathrm{ref}}}\right) \tag{3}$$

The Helmholtz potential is the logical choice because it represents the potential for work at constant volume and temperature. The volume of the adsorbed phase is fixed by the rigid zeolite lattice.

For systems with a small number of degrees of freedom, Z_N can be obtained by conventional importance sampling Monte Carlo integration with suitable choice of a biasing function (P).[29]

$$Z_N = \int_V \frac{\exp\left(\frac{-V}{kT}\right)}{P} P \, \mathrm{d}\vec{r}_1 ... \mathrm{d}\vec{r}_N \tag{4}$$

$$P = K \exp\left(\frac{-V^{\mathrm{com}}}{kT}\right) \tag{5}$$

The choice of biasing function is the key to doing this calculation quickly. We choose to use potentials that include only zeolite−sorbate interactions (V^{com}). In addition, the biasing potentials are defined to be constant throughout the volume of a cubelet. They take the value of the potential at one corner of the cubelet. This allows one to tabulate a grid of biasing functions for a given type of site. The constant K can be determined by requiring that P normalize to unity. Note that since the sorbate−sorbate interactions are neglected in the biasing function, the integral for the normalization can be separated into a product of integrals over each molecule's position space.

$$\int_V K \exp\left(\frac{-V^{\mathrm{com}}}{kT}\right) \mathrm{d}\vec{r}_1 ... \mathrm{d}\vec{r}_N = 1 = \prod_i^N \left[K_i \int_V \exp\left(\frac{-V_i^{\mathrm{com}}}{kT}\right) \mathrm{d}\vec{r}_i \right] \tag{6}$$

Here the notation i refers to separate, though indistinct, molecules within the volume V. To facilitate the computations, the quantity within the square brackets can be further required to normalize to unity. An expression for P then follows. Additionally, the integral can be simplified to a summation due to the discrete nature of V_i^{com}.

$$P = \prod_i^N \frac{\exp\left(\frac{-V_i^{\mathrm{com}}}{kT}\right)}{\int_V \exp\left(\frac{-V_i^{\mathrm{com}}}{kT}\right) \mathrm{d}\vec{r}_i} = \prod_i^N \frac{\exp\left(\frac{-V_i^{\mathrm{com}}}{kT}\right)}{\sum_{\mathrm{site}} \exp\left(\frac{-V_i^{\mathrm{com}}}{kT}\right) V_{\mathrm{cubelet}}} \tag{7}$$

The meaning of P is now clear. It is the probability density of finding N noninteracting molecules at a particular set of cubelet corners given that they can only occupy corners of cubelets. It should be noted that this biasing function is discrete and noninteracting, yet it still provides a sizable increase in computational efficiency. For example, a factor of 43 less CPU time is required per iteration with CF_4 in the zigzag channel of MFI.

The remainder of the computation is straightforward. A series of configurations is selected with probability $P \, \mathrm{d}\vec{r}_1 ... \mathrm{d}\vec{r}_N$ using the Metropolis Monte Carlo acceptance−rejection criteria. At each configuration the ratio of the integrand (see eqs 2 and 8) to the biasing probability is accumulated in a sum. When the simulation is finished, the sum is divided by the total number of configurations to produce the ensemble average of the integrand. The integral for the expectation energy can also be evaluated in the same manner and concurrently with the configurational integral.

$$\Delta U = \frac{\int_V V \exp\left(\frac{-V}{kT}\right) \mathrm{d}\vec{r}_1 ... \mathrm{d}\vec{r}_N}{Z_N} \tag{8}$$

Here the reference state is a noninteracting system at the same temperature and number of molecules. In general, if the reference state is noninteracting, such as an ideal gas, its V is zero. Therefore, Z_N^{ref} reduces to V^N, the configuration space volume of the collection of molecules. Once ΔU and ΔA are known, one can determine ΔS using $\Delta A = \Delta U - T\Delta S$. We will use ideal gas reference states here.

Computational time for this method is very small. Since both the potential that a sorbate would feel due to the zeolite and the probability P can be tabulated on grids, very little needs to be calculated on the fly. The zeolite−adsorbate potentials are interpolated from the grid, and the probabilities are used directly. Typically, a calculation converges within 100 000 to 1 million iterations and takes less than 1 min of CPU time on a 500 MHz single-processor workstation. This time includes the time necessary to tabulate the probability grid but not the potential grid. Runs of 100 million iterations were used to verify the convergence of the calculations.

GCMC Calculations

The energy-bias GCMC algorithm of Snurr et al.[31] was extended to handle multicomponent adsorption. Three kinds

of moves are implemented to sample the grand canonical ensemble. These are (1) translation moves, (2) attempts to insert a particle into the system, and (3) attempts to remove an existing particle from the system. The insertions are biased so that more attempts are made in the energetically favorable regions of the zeolite. This is done by discretizing the simulation volume into N_{cubelets} cubelets and then selecting a cubelet according to a weighting function. The weighting function, $\rho_i(n)$, is assigned to each cubelet n on the basis of the energy felt by sorbate i at the center of the cubelet. The weighting function is defined as

$$\rho_i(n) = \frac{\exp\left(\frac{-V_i(n)}{kT}\right)}{\sum_{j=1}^{N_{\text{cubelets}}} \exp\left(\frac{-V_i(j)}{kT}\right)} \tag{9}$$

where $V_i(j)$ is the sorbate−zeolite energy of a molecule of sorbate i at the center of cubelet j. An insertion of sorbate i is attempted by picking a cubelet n according to its weight and then placing the molecule at a randomly selected position within the cubelet. The insertion is accepted with probability min(1, P_{ins}), with

$$P_{\text{ins}} = \frac{1}{\rho_i(n)} \frac{V_{\text{cubelet}}}{V} \left\{ \frac{f_i V}{(N_i + 1)kT} \exp\left[\frac{-V}{kT}\right] \right\} \tag{10}$$

where V_{cubelet} is the volume of a cubelet, V is the volume of the simulation box, f_i is the fugacity of the sorbate i, N_i is the number of molecules of sorbate i in the simulation cell, and V is the potential energy of the molecule we are attempting to insert. The term in the curly braces is the acceptance probability for the standard GCMC without biasing. Since the insertions are biased, we must change the acceptance probability for deletion moves to preserve microscopic reversibility. Thus, the acceptance probability for a deletion move of a molecule of sorbate i from cubelet n is given by min(1, P_{del}), where

$$P_{\text{del}} = \rho_i(n) \frac{V}{V_{\text{cubelet}}} \left\{ \frac{N_i kT}{f_i V} \exp\left[\frac{-V}{kT}\right] \right\} \tag{11}$$

It is also important to perform the insertion and deletion moves for each component with equal probability to preserve microscopic reversibility. To ensure this, we followed the algorithm outlined by Karavias et al.[9] To test the validity of the algorithm and the acceptance criteria, we compared results obtained from biased and unbiased simulations of a CF_4/methane system at 10 atm. No discrepancy was found in the results. Snurr et al.[31] discuss the relative efficiency of biased versus unbiased GCMC.

The inputs to the simulation are the gas-phase fugacities of the components, the number of unit cells, and the temperature. The gas phase is assumed to be ideal so that the fugacities are simply given by the partial pressure of each component. The number of unit cells are chosen so that the edge lengths of the simulation cell are greater than 26 Å, since we use a 13 Å potential cutoff with periodic boundary conditions.[32] This corresponds to a size of 2 × 2 × 2 unit cells for MFI and 2 × 2 × 4 unit cells for MOR and BOG simulation cells. The production runs were 1 to 5 million steps long, where each Monte Carlo step consists of a translational step followed by either an insertion or a deletion step. Each subsequent point on an isotherm is generated by starting from the last configuration of the previous point for faster equilibration. The equilibration length of the simulation is discarded before doing the averaging. The statistical uncertainties were calculated by dividing each simulation run into 10 blocks and calculating the standard deviation of the block averages.

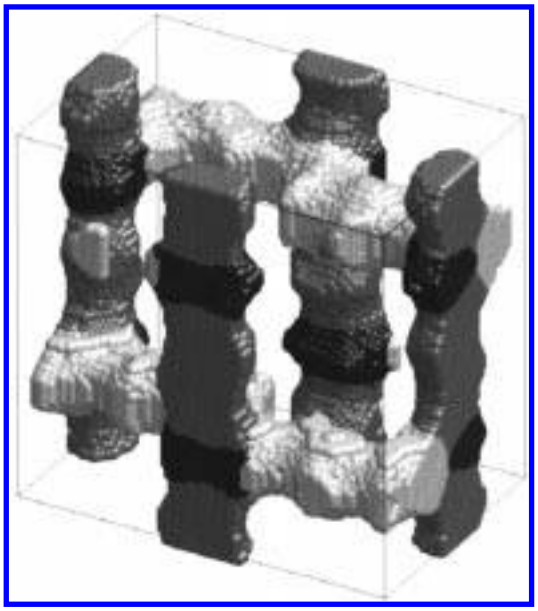

Figure 1. Site definitions for one unit cell of MFI. Shadings distinguish between sites (black, intersections; gray, straight channel; white, zigzag channel). Sites volumes are shown based on a 50 kJ/mol potential cutoff for the center of mass coordinate of argon. The surface is approximated as spheres to allow use of molecular visualization software.[22]

System Descriptions

Zeolites MFI, MOR, and BOG were chosen because they represent a good sampling of structures that each contain two sets of pores of different sizes and shapes. MFI is isomorphic with ZSM-5, an industrially important zeolite. Its largest uses are in catalytic applications that require high shape selectivity or low coking tendencies. It has orthogonal 10-ring pores, one straight (S) and one of zigzag shape (Z). The pores meet in intersections (I) that have a larger diameter than the pores themselves. Figure 1 shows the results of the site determination calculations for MFI using argon potentials. Crystallographic coordinates were taken from the work of Olson et al.,[33] who report pore dimensions of 5.4 × 5.6 Å for the straight channel and 5.1 × 5.4 Å for the zigzag channel. The relative pore volumes are I 13.0%, S 38.2%, and Z 48.8%. The total volume accessible to the argon center of mass at 50 kJ/mol is 885.2 Å^3/unit cell.

Figure 2 shows the site decompositions for MOR. Mordenite is also industrially important. It is typically used for alkylations, transalkylations, or other reactions that require a larger pore zeolite. It has 12-ring channels with 8-ring side pockets interspaced along their lengths. Mordenite also has flattened 8-ring channels that are impassable to the sorbates that we are studying here. These flattened 8-rings run parallel to the 12-rings and are accessed via the 8-ring side pockets. Only argon can access even part of these 8-ring channels, and still adsorption in these area makes up only ca. 1% of the total loading. Henceforth we will ignore the presence of this third site. Crystallographic coordinates were taken from the work of Alberti et al.[34] The relative pore volumes are side pockets 22.7% and 12-rings 77.3%. Notice that this zeolite, in contrast to MFI and BOG, is unidimensional. Adsorbates can only move in one direction as opposed to three. The total volume

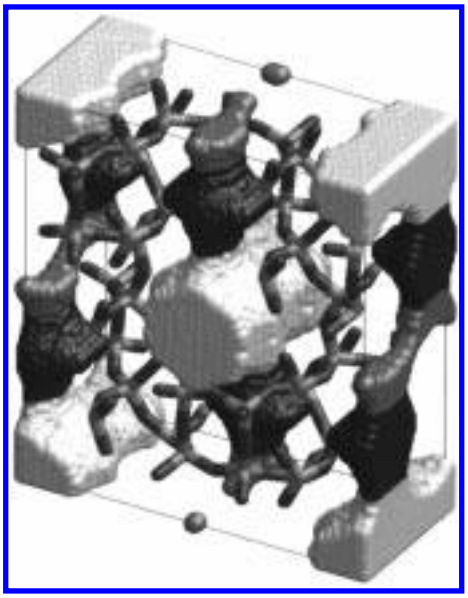

Figure 2. Site definitions for one unit cell of MOR. Shadings distinguish between sites (black, side pockets; gray, flattened 8-ring channel; white, 12-ring channel). The zeolite is displayed as sticks of silicon (light) and oxygen (dark). Sites volumes are shown based on a 50 kJ/mol potential cutoff for the center of mass coordinate of argon.

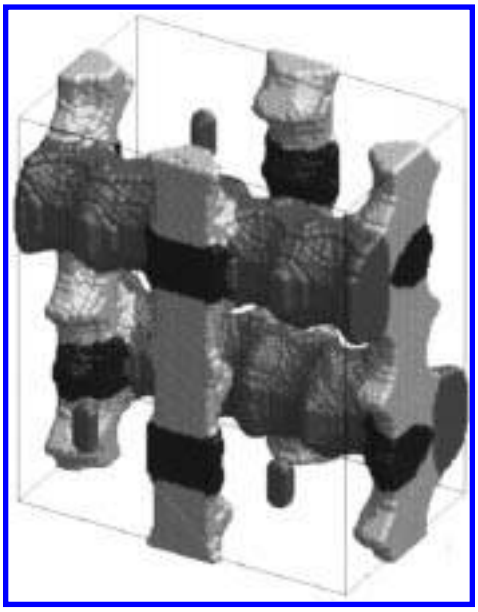

Figure 3. Site definitions for one unit cell of BOG. Shadings distinguish between sites (black, intersections; gray, 12-ring channel; white, 10-ring channel). Sites volumes are shown based on a 50 kJ/mol potential cutoff for the center of mass coordinate of argon.

accessible to the argon center of mass at 50 kJ/mol is 471.0 Å^3/unit cell. Pore dimensions were calculated using the method of Olson et al.[33] who assume a zeolite oxygen radius of 1.35 Å. The pore dimensions are 6.4 × 7.2 Å for the 12-ring, 3.4 × 4.8 Å for the 8-rings leading to the side pockets, and 1.1 × 5.7 Å for the flattened 8-ring channels.

Figure 3 shows that boggsite possesses intersecting 10-ring and 12-ring pores. Crystallographic coordinates were taken from the work of Pluth and Smith.[35] The relative pore volumes are I 10.3%, 12-rings 57.4%, 10-rings 32.3%. The total volume accessible to the argon center of mass at 50 kJ/mol is 1450.4 Å^3/unit cell. The pore dimensions are 6.9 Å for the 12-ring and 5.0 × 5.3 Å for the 10-rings. BOG is not used industrially because it is available only as a rare mineral and has not yet been synthesized. However, recently zeolites with similar

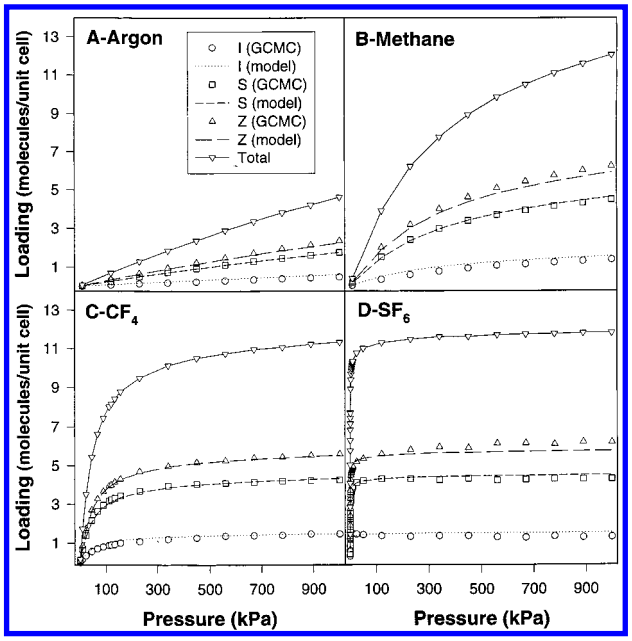

Figure 4. Adsorption isotherms at 300 K for argon (A), methane (B), CF_4 (C), and SF_6 (D) in zeolite MFI. The total loading points are shown, as well as loadings in each of the sites. The lines indicate the predictions of the volume-filling model. Good agreement between the model and the GCMC results indicates that the sites fill with minimal energetic preference. For all four adsorbates, the zigzag (Z) channels are the most preferred, as predicted at infinite dilution by the free energies in Table 2.

structures have been made. Lobo et al. have reported the synthesis of CIT-1,[36] which is believed to be identical to the B polymorph of SSZ-33.[37] SSZ-33 polymorphs and BOG have the same projection down the 12-ring pore and identical secondary building units. The fundamental difference lies in the way the units are connected. It is thought that this zeolite may possess useful shape-selective characteristics because of its unique combination of 10- and 12-ring pores.[38] It has also been tested as a cracking catalyst where it displays favorable activity and unusually high selectivity to isobutane.[39]

Single-Component Results

Grand canonical Monte Carlo simulations were used to generate single-component isotherms for the four sorbates in the three zeolites at 300 K. Figures 4−7 show the computed isotherms, including both total loading and the loading in each site. It is clear from these plots that the individual sites do not fill equally.

To explain the siting at low loadings, the energetics of the site/molecule combinations must be considered. Table 2 lists the free energies, potential energies, and entropies of infinite dilution molecule/site combinations at 300 K relative to an ideal gas. An arbitrary reference state of 30 atm, constant temperature, and number of molecules was chosen. The free energies can be used to understand the isotherms. At low loadings, the siting isotherms invariably follow the trends predicted by the free energy calculations. The lower the free energy in a site, the more the molecule prefers that site. For example, Figures 5 and 6 show that, at low loading, argon and methane adsorb preferentially in the side pockets of MOR, while CF_4 prefers the 12-ring channels.

The behavior at higher loadings generally does not follow the infinite dilution free energy trends. Naively one might expect each site to fill in proportion to its fraction of the total pore volume. Indeed, the MFI isotherms (Figure 4a−d) are

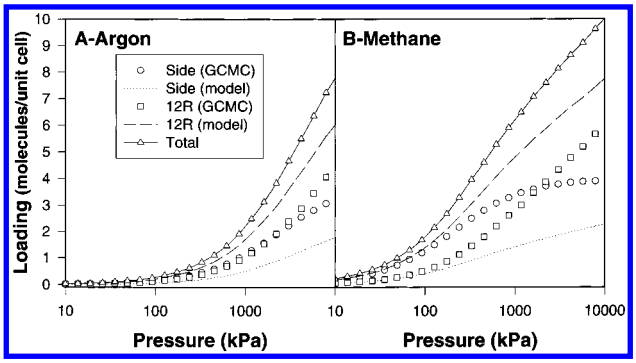

Figure 5. Adsorption isotherms at 300 K for argon (A) and methane (B) in zeolite MOR. The total loading points are shown, as well as loadings in each of the sites. The lines indicate the predictions of the volume-filling model. Comparatively poor agreement between the model and GCMC results indicates significant energetic preference in pore filling. For both adsorbates, the relative loadings at low total loading are well predicted by the free energies at infinite dilution in Table 2.

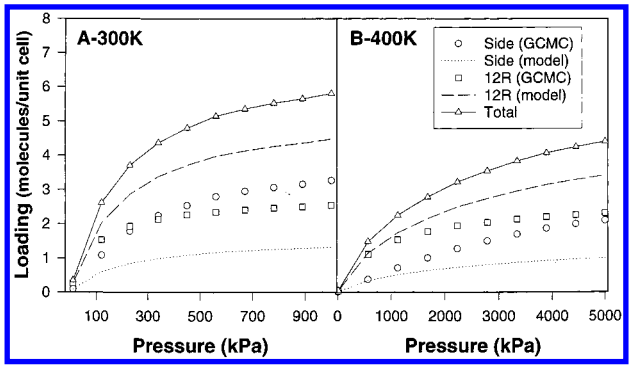

Figure 6. Adsorption isotherms for CF_4 at 300 K (A) and at 400 K (B) in zeolite MOR. The total loading curves are shown, as well as loadings in each of the sites. The lines indicate the predictions of the volume-filling model. Comparatively poor agreement between the model and GCMC results indicates significant energetic preference in pore filling. At both temperatures, the relative loadings at low total loading are well predicted by the free energies at infinite dilution in Table 2.

basically volume filling in this nature. Figures 4−7 also show, as lines, the predictions from this volume filling model. For MFI, across the entire range of loadings, the percent of molecules in each site varies from the volume percent of that site by less than a few percent. Similar agreement with the volume-filling model occurs only at very high pressures and loadings in some MOR and BOG systems. Argon and methane isotherms in MOR converge to the volume-filling model at 14 molecules/unit cell and 10×10^5 kPa. In BOG, convergence in the argon and methane isotherms is seen at 34 molecules/unit cell and 10×10^5 kPa. The CF_4 isotherms in MOR and BOG do not converge to the volume-filling model.

The driving forces behind the behavior at higher loadings are sorbate−sorbate interactions and site volume filling. These two effects work in opposition. At all but the very highest densities, sorbate−sorbate attractions lower the free energy. However, the dominant volume-filling effects decrease the entropy of adsorption and drive up the free energy. As more molecules fill a given site, the free energy difference associated with putting another molecule into that same site changes, becoming less favorable in all the situations we considered. The interaction of argon molecules with mordenite sites at 300 K (Figure 5) provides an example. Free energy calculations for more than one molecule in a unit cell's worth of side pockets or 12-rings were performed. The total argon free energy

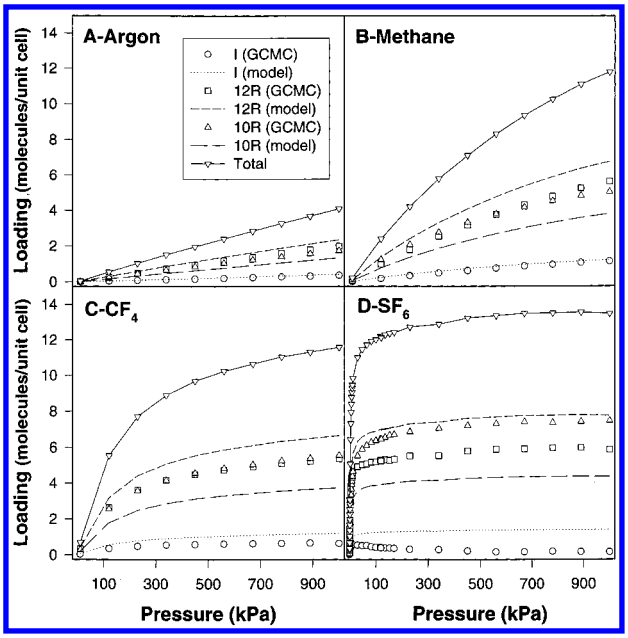

Figure 7. Adsorption isotherms at 300 K for argon (A), methane (B), CF_4 (C), and SF_6 (D) in zeolite BOG. The total loading curves are shown, as well as loadings in each of the sites. The lines indicate the predictions of the volume-filling model. Comparatively poor agreement between the model and GCMC results indicates significant energetic preference in pore filling. For all four adsorbates, the relative loadings at low total loading are well predicted by the free energies at infinite dilution in Table 2.

increase after addition of each new molecule is similar between the two sites (within 1 kJ/mol) up to five molecules/unit cell. By seven molecules/unit cell it is ca. 10 kJ/mol less favorable to insert an additional molecule into the side pockets than the 12-rings. When the site that is favored at infinite dilution begins to fill, the entropic effects suppress further adsorption in that site and result in adsorption into other sites. It is this *filling* tendency that makes the isotherms converge to the volume-filling model.

Not all the isotherms obey the volume-filling model at high loadings. A notable exception is the BOG/SF_6 isotherm, where at saturation loading a higher percentage of the molecules are in the *smaller* 10-ring sites than the 12-rings (Figure 7d). In such cases the ability of the adsorbate to pack into the individual sites becomes dominant in predicting the siting. Such *packing* effects have been observed previously at high loadings in idealized pores[18,40] and zeolite NaA.[13] In particular, it is not unusual for the adsorbed phase density to go through a maximum as the pore size is increased.[18] One of the more definitive indicators of packing effects is the sharpening of density distribution plots such as the radial distribution function. We invariably observed such localization at higher loadings in this work.

The isotherm for the MOR/SF_6 system is omitted because SF_6 is unlikely to access the side pockets of mordenite and therefore would display no interesting siting effects. Transport from the 12-ring channel to the side pocket was estimated to have a potential energy barrier of ca. 260 kJ/mol. CF_4 has a significantly lower barrier at 70 kJ/mol. If one assumes an Arrhenius hopping dependence with a preexponential factor of 10×10^{10} s^{-1}, then the rate is 6.5×10^{-3} s^{-1}. Such a rate is low, but significant, especially when one remembers that the energy barrier estimate was obtained using a rigid zeolite lattice. A real lattice is not rigid and may fluctuate enough to substantially affect the transport properties.[41] In addition it is

TABLE 2: Free Energies for Argon, Methane, CF_4, and SF_6 in Each Site of Zeolites MFI, MOR, and BOG at 300 K[a]

zeolite−sorbate	site	ΔA (kJ/mol)	ΔU (kJ/mol)	ΔS (J/mol/K)	Z_N (Å^3)
MFI−argon	I	−1.6	−9.1	−25.1	2.54×10^3
	S	−5.2	−10.3	−17.3	1.08×10^4
	*Z	−5.6	−10.3	−15.7	1.29×10^4
MFI−methane	I	−5.8	−13.7	−26.5	1.39×10^4
	S	−10.0	−15.8	−19.3	7.59×10^4
	*Z	−10.4	−15.8	−17.9	8.93×10^4
MFI−CF_4	I	−10.5	−20.1	−32.1	9.21×10^4
	S	−14.0	−22.7	−28.8	3.74×10^5
	*Z	−14.2	−22.6	−28.1	4.00×10^5
MFI−SF_6	I	−23.5	−34.7	−37.4	1.67×10^7
	S	−24.2	−35.1	−36.4	2.20×10^7
	*Z	−24.6	−35.5	−36.5	2.56×10^7
MOR−argon	*side	−3.9	−13.4	−31.8	6.52×10^3
	12R	−3.4	−8.0	−15.4	5.34×10^3
MOR−methane	*side	−10.0	−20.4	−34.8	7.59×10^4
	12R	−7.2	−12.2	−16.7	2.39×10^4
MOR−CF_4	side	−8.4	−24.2	−52.8	3.89×10^4
	*12R	−11.4	−17.9	−21.6	1.34×10^5
BOG−argon	I	−0.6	−7.4	−22.5	1.74×10^3
	12R	−4.8	−7.1	−7.9	9.19×10^3
	*10R	−4.8	−9.3	−15.0	9.37×10^3
BOG−methane	I	−4.0	−11.4	−24.4	6.89×10^3
	12R	−8.1	−10.9	−9.3	3.49×10^4
	*10R	−9.2	−14.5	−17.7	5.44×10^4
BOG−CF_4	I	−7.2	−15.3	−27.3	2.42×10^4
	12R	−11.7	−15.7	−13.2	1.47×10^5
	*10R	−11.8	−19.5	−25.7	1.52×10^5
BOG−SF_6	I	−17.0	−26.2	−30.6	1.23×10^6
	*12R	−22.3	−27.6	−17.8	1.03×10^7
	10R	−19.6	−28.6	−29.8	3.56×10^6

[a] Each integration volume is composed of all sites of a given type within a single unit cell. Free energies, potential energies, and entropies are reported relative to an ideal gas at 30 atm and at constant temperature and number of molecules. An asterisk (*) indicates the thermodynamically favored site at infinite dilution.

known that CF_4 does adsorb into other 8-ring pore zeolites such as zeolite 4A and 5A.[42] We therefore predict that CF_4 would be able to access the side pockets of MOR. The potential energy barriers for entry of argon and methane into the side pocket site are substantially lower and clearly pose no difficulties to entry.

The heterogeneity of a zeolite structure can noticeably affect adsorption isotherms. In extreme cases one may see a step when one site fills first and only then is followed at higher pressures by significant filling in other sites. Figure 8 shows a step in the argon in boggsite isotherm at 80 K. Adsorption in the intersection has a free energy of −7.4 kJ/mol compared to −8.0 kJ/mol in the 12-rings and −9.8 kJ/mol in the 10-rings. The 10-rings, since they have the lowest free energy at 80 K, fill first. The intersections and 12-rings fill significantly only at higher pressures, and the result is a step. Adsorption of argon in mordenite at 80 K is similar. In mordenite, the reason for this delayed filling stems from the sizable energetic differences between the side pocket and the 12-ring sites. The potential energy minima are −22 and −15 kJ/mol, respectively, with the potentials used here. Macedonia et al.[43] have observed a step in this system using GCMC techniques and confirmed it experimentally. Our simulation results agree well with theirs and so are not shown here.

The steps in the isotherms of argon in MOR and BOG are predominately caused by one site having a significantly lower

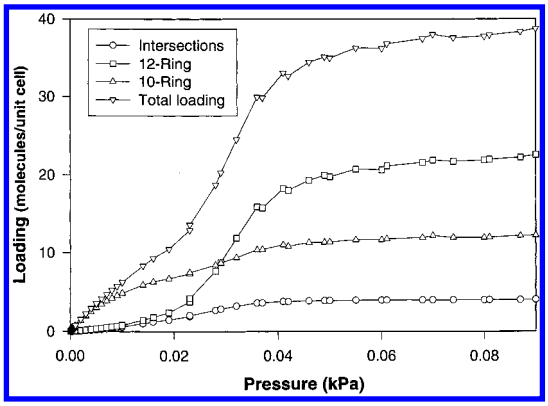

Figure 8. Adsorption isotherm for argon in boggsite at 80 K. The step is due to the potential energy induced preferential filling of the 10-ring channels before the other sites.

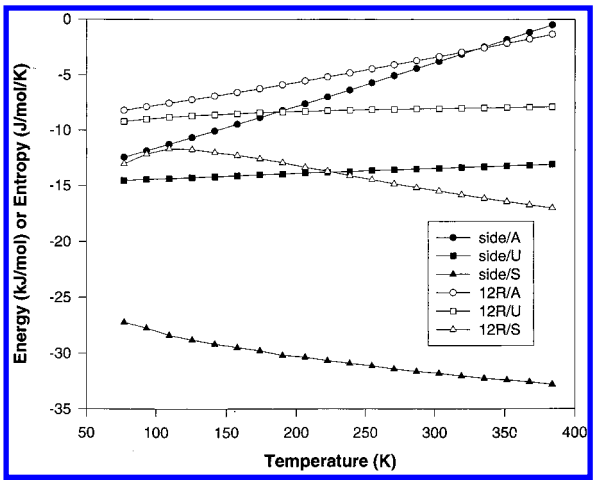

Figure 9. Variation in the infinite dilution Helmholtz free energies, potential energies, and entropies for argon in mordenite as a function of temperature. Separate curves are shown for the 12-ring sites and the side pockets. The adsorption free energy difference between the sites is greatest at lower temperatures.

potential energy for adsorption than the others. At 80 K, entropy effects do not play a significant role, but at higher temperatures the effect of entropy becomes greater. The infinite dilution free energy, potential energy, and entropy for argon in the sites of MOR can be seen in Figure 9 as a function of temperature. At 80 K the free energy difference between adsorption in the two sites is significant (4.2 kJ/mol), contributing to a step in the isotherm. It is only at low temperatures that differences in entropy become unimportant enough to allow the potential energy differences to dominate the free energy. Clearly there is no step in the 300 K isotherm at low loadings (Figure 5a). None are seen at higher loadings because neither site is filling significantly more than the other.

Figure 9 has other interesting features worth mentioning. It can be seen that the entropy in the 12-ring pores goes through a maximum near 100 K, while that in the side pockets monotonically decreases. This entropy maximum is not unusual in the systems studied here. It coincides with a small positive curvature in the potential energy. Changes in the potential energy are caused by the molecule spending more time in higher energy portions of the site as the temperature increases. Since the higher energy portions of the zeolite are closer to the zeolite atoms, the volume accessible to the molecule effectively increases. When the volume increases, the entropy also increases, explaining the initial entropy increase. Since the free energy is referenced to an ideal gas, whose expansion is not

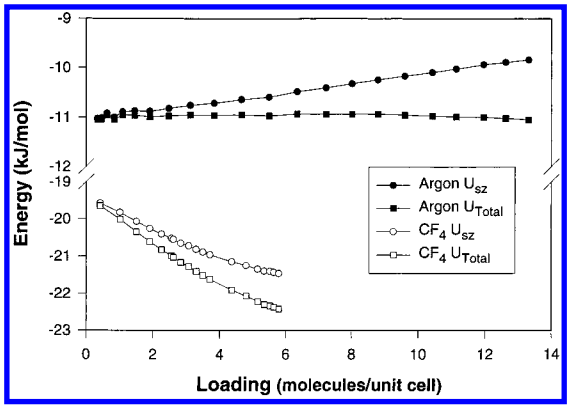

Figure 10. Average potential energy per molecule for argon and CF_4 single-component systems in MOR at 300 K. The zeolite−sorbate contribution and the total are shown separately. The distance between the zeolite−sorbate curve and the total represents the sorbate−sorbate contribution to the energy.

limited by the zeolite pore walls, the adsorption entropy eventually decreases. The result is the maximum observed.

The presence of large differences in entropy between adsorption in two sites raises the possibility that siting could be dictated largely by entropy effects in some systems. In an extreme case this might again cause a step in an isotherm. At low temperatures, the steps discussed above were primarily due to large potential energy differences between sites. At higher temperatures, large entropy differences could produce enough of a free energy difference to produce a step. The MOR/CF_4 system might be a likely candidate for this effect. CF_4 is large enough that one might expect it to be more favored in the 12-rings than the side pocket. Table 2 free energies indicate that at 300 K this is the case. However, Figure 6a does not show a step in the overall isotherm. At 400 K the difference in free energies between the two sites is even larger than that at 80 K in the MOR/argon system (6.1 vs 4.2 kJ/mol), yet Figure 6b shows no step. The greater effect of entropy does seem to inhibit the adsorption of CF_4 into the side pockets. It is not enough, however, to cause a step because the higher temperature decreases adsorption and tends to smooth the isotherm.

The order in which sites are filled influences the way that the heat of sorption varies with loading. Figure 10 shows the average potential energy per molecule as a function of loading for argon and CF_4 single-component systems in mordenite at 300 K. Most notable is the *decrease* seen in the CF_4 sorbate−zeolite potential energy in contrast to the *increase* for argon. From Figure 5, one sees that, at low pressures, argon fills the side pockets and 12-ring channels simultaneously. From Table 2, the potential energies for the sites are −13.4 and −8.0 kJ/mol, giving an average in agreement with the zeolite−sorbate energy seen in Figure 10 at low loading. As the side pockets reach saturation, a higher fraction of molecules are adsorbed in the 12-ring channels, causing the rise in zeolite−sorbate energy with loading. Attractive argon−argon interactions compensate, causing the total energy to be relatively constant with loading. Similar trends have been reported previously, for example, in the methane in silicalite system.[44]

The results for CF_4 in mordenite look quite different. The zeolite-sorbate energy *decreases* with increased loading. Because of the significant entropic penalty to adsorption in the side pockets, CF_4 adsorbs first in sites of higher potential energy (the 12-ring channels) and only at higher loadings fills the enthalpically preferred side pockets. Attractive sorbate−sorbate interactions result in a total energy that also decreases with loading.

TABLE 3: Adsorbed Phase Site Compositions in Equilibrium with a 50/50 Gas-Phase Mixture of Methane and CF_4 at 10 atm and 400 K[a]

zeolite	site	methane (%)	CF_4 (%)
MFI	I	26.5	73.5
	S	30.7	69.3
	Z	31.8	68.2
	overall	**30.7**	**69.3**
MOR	side	72.2	27.8
	12R	27.7	72.3
	overall	**47.0**	**53.0**
BOG	I	34.1	65.9
	12R	30.5	69.5
	10R	38.6	61.4
	overall	**34.1**	**65.9**

[a] The MOR system displays large local deviations from the overall composition, while the MFI and BOG systems do not.

The results of Figure 10 have important implications for interpretation of experimental heats of adsorption in microporous materials. When the heat becomes less favorable with increased loading, this is often interpreted as a sign of energetic heterogeneity. Increasingly favorable heats with increased loading are then attributed to sorbate−sorbate attractions. However, applying this interpretation to the total energy curves of Figure 10 (e.g., if they were experimental data) would lead to an incorrect interpretation. The more heterogeneous system, CF_4/MOR, shows a decrease in energy with loading, not an increase. This unusual result is a direct result of the entropic penalty for adsorption in the side pockets, which causes the less enthalpically favored sites to be filled first. When micropores are present, the possibility of this kind of behavior must be considered.

Binary Results

Binary adsorption was also investigated using GCMC. Preferential siting is again observed, resulting in some cases in segregation of different species of a mixture into different regions of the zeolite pores. Table 3 shows results for adsorption of a 50/50 gas-phase mixture of methane and CF_4 at 10 atm and 400 K in the three zeolites. In mordenite, the entropic penalty to adsorption of CF_4 in the side pockets leads to substantial segregation. 72.2% of the molecules in the side pocket are methane, and 72.3% of the molecules in the 12-rings are CF_4. In contrast, much smaller deviations from the overall composition are observed in the MFI and BOG sites. This system might be amenable to experimental verification. It may be possible to measure the segregation using chemical shift measurements or cross-polarization between the ^1H and ^{19}F nuclei in NMR experiments.

The *filling* and *packing* models used in the previous section are also effective here. Indeed, in energetically homogeneous systems such as argon and methane in zeolite MFI the siting does obey the volume-filling model. Yet, the simple models do not complete the picture because there are now multiple species with different energetics present in the same structure. We have chosen to use variable gas-phase composition simulations at constant temperature and pressure to emphasize the effects of sorbate−sorbate interactions. The binary combinations of the four sorbates and three zeolites (excluding SF_6 in MOR) were investigated using GCMC. Constant pressures of 1 and 10 atm were chosen to provide data under atmospheric conditions and to look at adsorption under high loading situations. It became apparent that the systems follow trends that could be reduced to four qualitative models, *volume filling*,

competition, *reconciliation*, and *accommodation*. Consequently, it will only be necessary to show enough of the results to illustrate the models.

Again, it is helpful to return to the infinite dilution free energies to help describe the adsorption phenomena. Table 2 shows that the free energies of a species in a particular site decrease monotonically with molecule size in most cases. For example, the sequence $SF_6 < CF_4 <$ methane < argon holds in the intersection (I) site of MFI with SF_6 being the most favored adsorbate. Also note that each species has a site that it thermodynamically favors at infinite dilution. This site will be referred to as the "favored" site of the species.

It should be noted again that the free energy values in Table 2 are those for only one molecule in a site. Since the calculations were done at infinite dilution, they do not include effects from the presence of additional molecules of the same species or nearby dissimilar molecules. Consequently, the reported free energies can only be used as qualitative indicators of trends at higher loadings. Free energies at higher loadings could be calculated, but the number of situations to be considered and the complexity of the calculations increase quickly.

The decrease of the free energy with increasing size of the molecule in a given site is not a universal trend. If the site is small enough, confinement effects can substantially decrease the entropy of a larger molecule and make adsorption in that site unfavorable despite a low potential energy in the site. Such a situation is seen for CF_4 in MOR (see previous section). There is a large entropic penalty for CF_4 adsorption in the side pockets. It should be mentioned that there may also be quantum mechanical barriers to adsorption in a small site. Beenakker[45] et al. have proposed that confinement of a molecule's wave function may be sufficient to raise its zero-point energy significantly.

Frequently the two components of a binary mixture may both be favored in the same site, according to the infinite dilution free energies. The argon/methane/MFI system is an example. One would expect that in a competition for occupancy of the favored site, the species that has the lowest free energy (usually the largest) will segregate into that site. Consequently, the other (usually smaller) species will be displaced from that site into one in which it has a higher free energy. This *competition* model is one of the most common. It was also observed by Karavias and Myers in a CO_2/methane/FAU system, where regions near cations were the most favored sites.[9]

The argon/methane/MOR system also illustrates the competition model. Figure 11a shows the loading in each site for both species at 10 atm and 300 K. Notice that the argon/side pocket line dips below the argon/12R line when the methane begins to adsorb. Methane is displacing the argon because it has a lower free energy in the side pockets. Xu et al.[7] observed similar segregation of methane into the side pockets at 4−100 K in a methane-rich argon−methane mixture. Figure 11b makes the trend more apparent. The argon/side pocket and argon/12R lines separate more and more until at high gas-phase mole fraction of methane, 70% of the argon is in the 12-ring sites, its less favored site. The percent of the methane in the side pocket decreases because methane must also begin to go into the 12-rings as the side pockets fill.

In a system where the two species do not thermodynamically favor the same site, there is no competition. The argon/CF_4/MOR system at 300 K and 10 atm, shown in Figure 12, is an example. It is clear that at low total loadings both species are segregated into their thermodynamically favored sites: argon

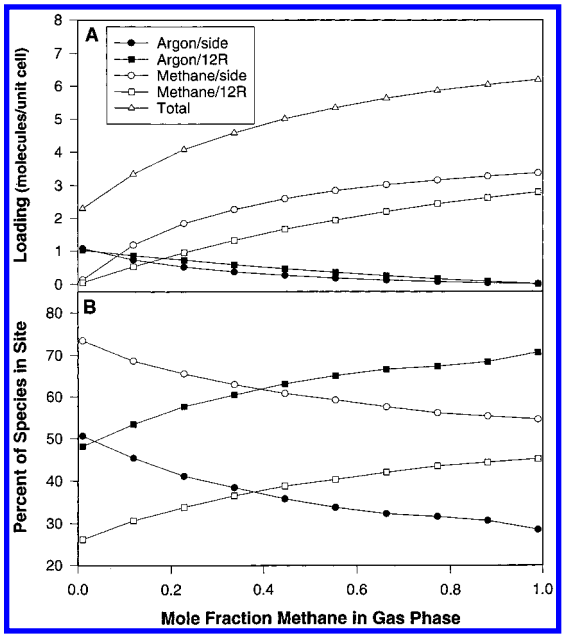

Figure 11. Variable gas-phase composition adsorption of argon and methane in MOR at 300 K and 10 atm. The data are shown in terms of loading per site (A) and in terms of percent of each species per site (B). Argon and methane compete for the side pocket sites and methane dominates (competition model).

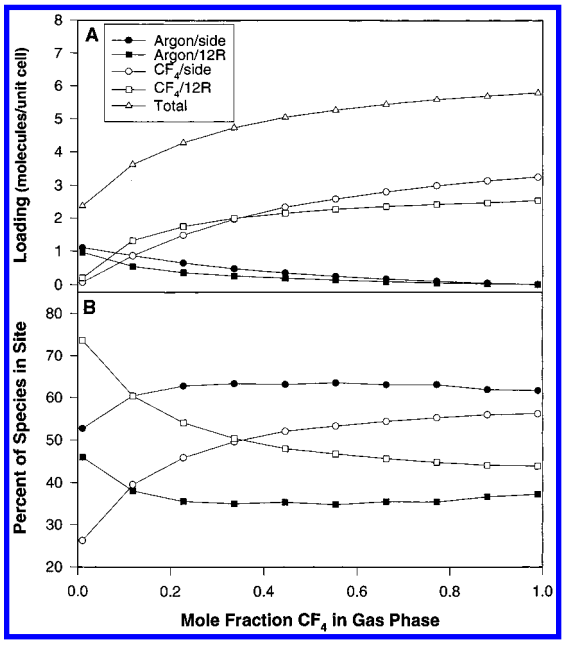

Figure 12. Variable gas-phase composition adsorption of argon and CF_4 in MOR at 300 K and 10 atm. The data are shown in terms of loading per site (A) and in terms of percent of each species per site (B). Argon and CF_4 are favored in the side pocket and 12-ring sites, respectively. Here there is no competition for adsorption sites (reconciliation model).

adsorbs preferentially in the side pockets and CF_4 in the 12-rings. This situation is termed the *reconciliation* model. The crossing of the two CF_4 lines is due to filling effects in the 12-rings. The contrast between Figures 11b and 12b is substantial. Together they imply that a reversal in argon siting can occur simply owing to the presence of a different coadsorbate. The methane/CF_4/MOR system (not shown) also behaves according to the reconciliation model.

In some cases each species selectively adsorbs in the site that both favor. When argon and methane are coadsorbed in MFI

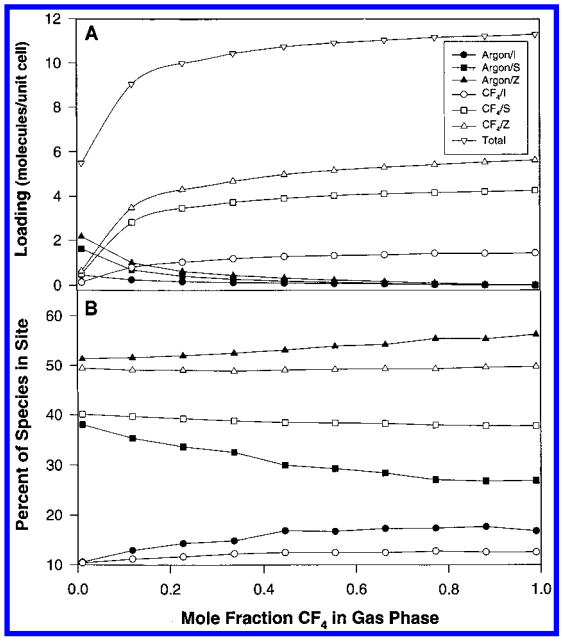

Figure 13. Variable gas-phase composition adsorption of argon and CF_4 in MFI at 300 K and 10 atm. The data are shown in terms of loading per site (A) and in terms of percent of each species per site (B). Argon and CF_4 are both favored in the zigzag channels, yet the percent of both in this site increases as the gas-phase CF_4 mole fraction is increased. This is contrary to the expectation that CF_4 will displace argon in the favored zigzag channels owing to its lower free energy in that site (accommodation model).

both species prefer the zigzag channels. The percent of each species in this site is identical to the volume percent of the site across the entire range of gas-phase compositions. Thus, this system obeys the volume filling model.

If the presence of an additional component were to push the other species *more* into its favored site, then new effects would be present. Such a system is said to obey the *accommodation* model. It can be thought of as the counterpart to the competition model when the species cooperate instead of compete to occupy the same site. The argon/CF_4/MFI system is a mild example of this model. Figure 13 shows that the percent of argon in its favored zigzag (Z) site increases slightly as more CF_4 is adsorbed. In addition, the percent in the intersections increases, while the percent in the straight (S) channels decreases. As the CF_4 loading increases, there may be more open spaces accessible to argon in the intersections than in the straight channels owing to packing effects.

The exact cause of the accommodation phenomenon is not entirely clear. However, it is likely that the larger species packs into the site in such a way that spaces remain open to the smaller species. Figure 14a shows two probability density contour plots made from data accumulated during GCMC simulations of the argon/CF_4/MFI system in Figure 13. Figure 14a corresponds to the fourth point from right in Figure 13, at 66.3% CF_4 in the gas phase. The adsorbed phase composition is 0.29 argon/unit cell and 10.77 CF_4/unit cell. By comparing the 50% probability density contours of CF_4 (black) and argon (light gray), one can see that the argon tends to prefer the regions close to the pore walls in the same areas that the CF_4 prefers. It can also be seen that the argon is able to pack between the CF_4 molecules in high probability density areas. Figure 14b is for the single-component CF_4/MFI system. Comparison of parts a and b of Figure 14 allows one to conclude that the argon does not affect the CF_4 placement. A similar plot of an argon system without the CF_4 indicates that the argon *is* affected by the presence of the CF_4.

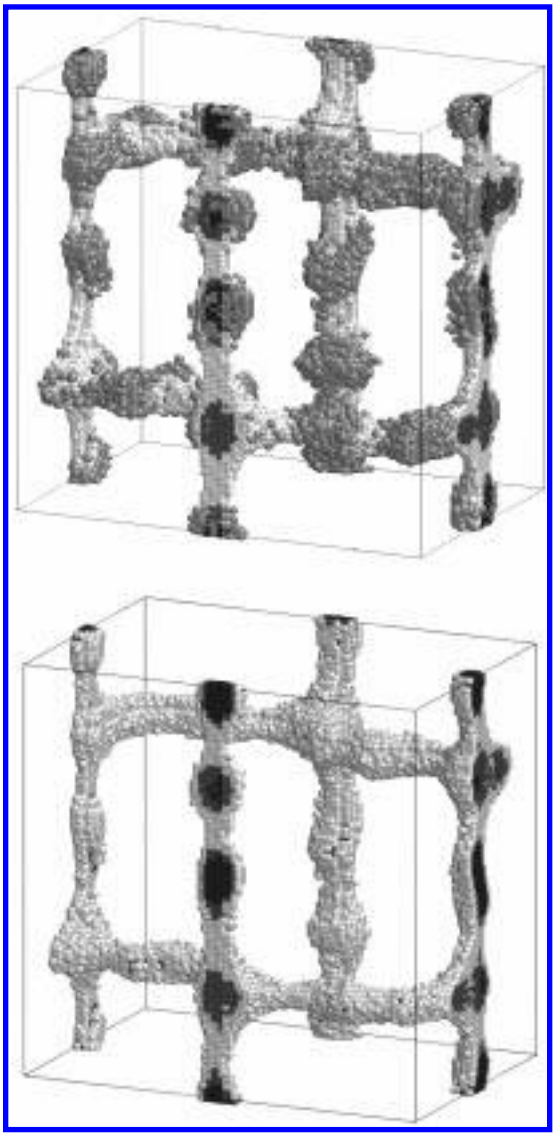

Figure 14. Probability density contour plots for argon/CF_4/MFI (A, top) or CF_4/MFI (B, bottom) at 300 K and 10 atm. The different degrees of shading represent volumes that enclose the most probable adsorption locations. For example, the black volume encloses the most likely 50% of the positions occupied by the CF_4 molecules (dark gray, 80% CF_4; white, 100% CF_4; light gray, 50% argon). The contours are displayed such that volumes enclosing smaller percents overlay higher percent contours. In addition, the argon contour overlays all others and is directly comparable to the black CF_4 contour. The rough nature of the contours is due to discretization of the points and finite nature of the simulation. Comparing parts B and A indicates that the CF_4 is unaffected by the presence of the argon at low loading.

The physical picture behind these contour plots is that the CF_4 (larger species) packs into the pore structure without regard for the argon. Argon is then forced to pack into the spaces unwanted by the CF_4. In this case these spaces are near the pore wall and between the CF_4 molecules. The accommodation phenomenon is due to the remaining spaces in the zigzag channels and intersections being more favorable than those in the straight channels.

The remainder of the MFI data not displayed can be summarized easily. When argon and methane are coadsorbed at 10 atm and 300 K, they essentially obey the volume-filling model across the full range of compositions. Both species are preferred in their infinite dilution favored sites. When methane and CF_4 are coadsorbed at 10 atm and 300 K, both species are again preferred in their favored sites with little change over the

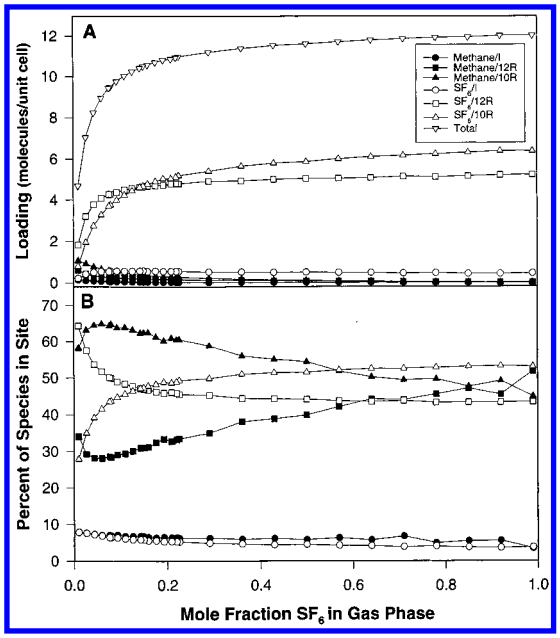

Figure 15. Variable gas-phase composition adsorption of methane and SF_6 in BOG at 300 K and 1 atm. The data are shown in terms of loading per site (A) and in terms of percent of each species per site (B). Methane and SF_6 are favored in the 10-rings and 12-rings, respectively, at infinite dilution. The presence of SF_6 displaces methane more into its favored site at low loading than expected from the single-component methane isotherm (reconciliation model).

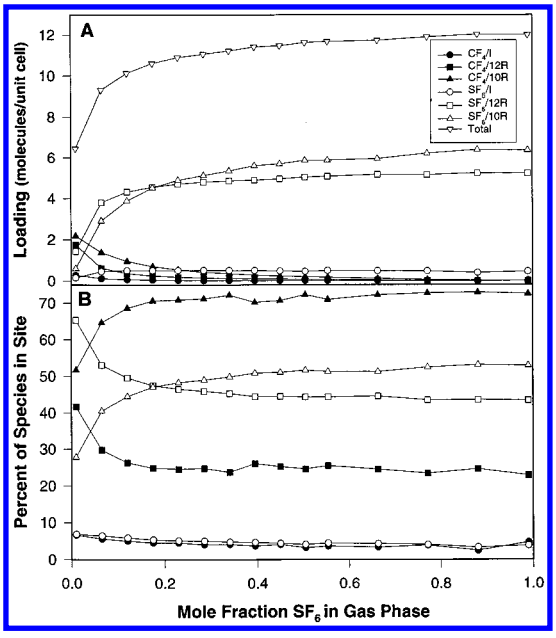

Figure 16. Variable gas-phase composition adsorption of CF_4 and SF_6 in BOG at 300 K and 1 atm. The data are shown in terms of loading per site (A) and in terms of percent of each species per site (B). Here CF_4 is encouraged to reside in the 10-ring sites it favors at infinite dilution by the presence of SF_6 (reconciliation model).

composition range. However, the volume-filling model is no longer strictly obeyed. Methane is adsorbed slightly more into the zigzag channels than the volume-filling model predicts. This system is therefore another mild example of the accommodation model. For the systems having SF_6 as a coadsorbate, very little of the smaller component is adsorbed.

Boggsite systems can also be characterized by the four models, though not as clearly. Figure 15 shows the methane/SF_6/BOG system at 300 K and 1 atm. At low gas-phase mole fraction of SF_6, both species segregate into their favored sites, methane into the 10-rings and SF_6 into the 12-rings. In this system, a larger percent of the methane is in the 10-rings than seen in the pure component system at the same loading. The site placement of the SF_6 is unaffected by the presence of the methane; the pure component isotherm shows exactly the same siting behavior. This system obeys the reconciliation model best because the presence of SF_6 pushes the methane more into its favored site.

At higher loadings, the methane/SF_6/BOG system is more difficult to fit into the four models. As the zeolite fills with SF_6, the extent of methane segregation decreases until there is no preference between the 10-ring and 12-ring channels. The odd packing tendency of the SF_6 has pushed the methane out of the 10-ring channel even though the 10-ring is not the favored site of SF_6.

If the methane is exchanged for CF_4 the segregation trends change. Figure 16 shows a CF_4/SF_6/BOG system at 1 atm and 300 K; the 10 atm system is similar. This system is a clear example of the reconciliation model. As a single component, CF_4 never displays more than a 5% difference between the percent of species in 12-ring and 10-ring sites. Coadsorbed with SF_6, the percentage of CF_4 molecules in the 10-ring channels is around 40% higher than in the 12-ring channels across most of the composition range.

In other boggsite systems, segregation effects are also seen. When argon is present in a BOG system it is consistently displaced into the 12-rings by the larger species. The methane/CF_4/BOG system displays siting no different from the pure component isotherms. This is probably because differences in their sizes and free energies are not large enough to provide a driving force for significant segregation.

Conclusions

The intention of this work was to investigate siting and segregation of simple adsorbates in single-component and binary zeolite systems. As expected, siting preferences are due to free energy differences between adsorption in different sites. What is now clearer are the individual roles that potential energy and entropic contributions play, especially at higher loadings. The free energy calculations performed here provide a fast method for predicting the sitings at low loadings and a good basis for studying the segregation at higher loadings. Decomposition of the free energies into potential energies and entropies provides a good method for comparing adsorption in the three zeolite structures. It seems that, despite the differences between real pores and idealized slits, cylinders or spheres, such ideal work is generally applicable to more realistic systems.

In MFI, the intersections are comparatively unfavorable owing to a high potential energy and low entropy. Adsorption in the straight or zigzag channels have very similar potential energies. The zigzag channel is slightly more favored due to its higher entropy. Consequently, MFI provides a more energetically homogeneous environment than MOR or BOG. As a result, single-component adsorption in MFI largely obeys the *volume-filling* model. In binary MFI systems, only mild segregation is observed, perhaps because the relatively similar shapes of the pores do not encourage formation of significantly different spaces between molecules of the strongly adsorbed species.

Adsorption in MOR is strikingly different. Since MOR possesses two sites of very different sizes, the free energies for adsorption in these sites are also very different. This heterogeneity results in substantial deviations from the volume-filling model. Adsorption in the side pockets has a much lower

potential energy, yet in some cases confinement decreases the entropy of adsorption in the side pocket so much that it is thermodynamically unfavored. This concept of an entropic penalty should be quite applicable to other sorbate/zeolite pairs, including larger, more complex molecules.

Boggsite systems are more complex. The dissimilarly sized channels do lead to significantly different free energies of adsorption, though not to the extent seen in MOR. The potential energy for adsorption is lowest in the 10-ring channels for all four molecules. This leads, at 300 K, to the 10-ring channel being the most favored site at infinite dilution for all but SF_6. SF_6 is large enough so there is a significant entropic penalty for adsorption in the 10-ring channel. The result is that SF_6 is favored in the 12-ring channel at low loadings. At higher loadings, packing effects dominate and the SF_6 placement reverses. The energetic heterogeneity and the presence of packing effects result in substantial deviations from the volume-filling model. The binary systems in BOG are more complex than in MFI or MOR, presumably because packing effects that are difficult to predict without simulations are more important.

Some general conclusions can be made about segregation of the binary combinations of the four species in MFI, MOR, and BOG. It seems that the more weakly adsorbed species has comparatively little effect on the positions of the strongly adsorbed species. The greater the difference in free energies of adsorption, the more this is true. For the four molecules considered here, larger molecules almost invariably have lower free energies in all sites than their smaller counterparts. The result, in general, is the creation of spaces between and around the larger species. The characteristics of these spaces then determine the segregation of the smaller, more weakly adsorbed species and therefore differentiate between volume-filling, competition, reconciliation, and accommodation phenomena. It is expected that similar effects will be observed in other binary sorbate/zeolite systems.

Significant segregation does occur even in systems with simple spherical molecules. We expect that for more complex molecules the shape of the site and the molecular conformation will become more important in determining free energies and therefore segregation. For this reason, segregation effects are expected to influence some significant fraction of adsorption systems, in particular ones containing strong heterogeneity in their pore structures. The possibilities for better understanding of adsorption and for better control of catalytic reactions justify further work in this area.

Additional Note

While this article was in review it came to our attention that the zeolite−sorbate potentials used for SF_6 could be improved upon. Readers interested in potential model development should note that the SF_6 potentials used here overpredict the Henry's constant for SF_6 in silicalite and underpredict the saturation loading.[16]

Acknowledgment. The authors gratefully acknowledge helpful discussions with Prof. E. J. Maginn. Acknowledgment is made to the donors of the Petroleum Research Fund, administered by the American Chemical Society, for partial support of this research.

References and Notes

(1) Yan, Y.; Bein, T. *J. Am. Chem. Soc.* **1995**, *117*, 9990−9994.
(2) Pereira, C.; Hash, M.; Lewis, M.; Richmann, M. *JOM* **1997**, *49*, 34−37.
(3) Funke, H. H.; Argo, A. M.; Falconer, J. L.; Noble, R. D. *Ind. Eng. Chem. Res.* **1997**, *36*, 137−143.
(4) Leibovitch, M.; Olovsson, G.; Sundarababu, G.; Ramamurthy, V.; Scheffer, J. R.; Trotter, J. *J. Am. Chem. Soc.* **1996**, *118*, 1219−1220.
(5) Dunne, J. A.; Rao, M.; Sircar, S.; Gorte, R. J.; Myers, A. L. *Langmuir* **1997**, *13*, 4333−4341.
(6) Karavias, F.; Myers, A. L. *Langmuir* **1991**, *7*, 3118−3126.
(7) Xu, Q.; Eguchi, T.; Nakayama, H.; Nakamura, N. *J. Chem. Soc., Faraday Trans.* **1996**, *92*, 4601−4603.
(8) Ripmeester, J. A. *J. Am. Chem. Soc.* **1982**, *104*, 289−290.
(9) Karavias, F.; Myers, A. L. *Mol. Simul.* **1991**, *8*, 51−72.
(10) Razmus, D.; Hall, C. *AIChE J.* **1991**, *37*, 769−779.
(11) Maddox, M.; Rowlinson, J. *J. Chem. Soc., Faraday Trans.* **1993**, *89*, 3619−3621.
(12) Dunne, J.; Myers, A. *Chem. Eng. Sci.* **1994**, *49*, 2941−2951.
(13) Van Tassel, P. R.; Davis, H. T.; McCormick, A. V. *Langmuir* **1994**, *10*, 1257−1267.
(14) Van Tassel, P. R.; Davis, H. T.; McCormick, A. V. *Mol. Simul.* **1996**, *17*, 239−254.
(15) Jameson, C. J.; Jameson, A. K.; Lim, H. M. *J. Chem. Phys.* **1996**, *104* (4), 1709−1728.
(16) Dunne, J.; Mariwala, R.; Rao, M.; Sircar, S.; Gorte, R.; Myers, A. *Langmuir* **1996**, *12*, 5888−5895.
(17) Heuchel, M.; Snurr, R. Q.; Buss, E. *Langmuir* **1997**, *13*, 6795−6804.
(18) Keffer, D.; Davis, H. T.; McCormick, A. V. *J. Phys. Chem.* **1996**, *100*, 638−645.
(19) Van Tassel, P. R.; Davis, H. T.; McCormick, A. V. *AIChE J.* **1994**, *40*, 925−934.
(20) Bird, R. B.; Stewart, W. E.; Lightfoot, E. N. *Transport Phenomena*; John Wiley & Sons: New York, 1960.
(21) Reid, R. C.; Prausnitz, J. M.; Poling, B. E. *The Properties of Gases and Liquids*, 4th Ed.; McGraw-Hill: New York, 1987.
(22) Sayle, R.; Milner-White, E. J. *Trends Biochem. Sci.* **1995**, *20*, 374.
(23) Kiselev, A. V.; Lopatkin, A. A.; Shulga, A. A. *Zeolites* **1985**, *5*, 261−267.
(24) Snurr, R. Q.; Kärger, J. *J. Phys. Chem. B* **1997**, *101*, 6469−6473.
(25) Smit, B. *J. Phys. Chem.* **1995**, *99*, 5597−5603.
(26) June, R. L.; Bell, A. T.; Theodorou, D. N. *J. Phys. Chem.* **1991**, *95*, 8866−8878.
(27) Snurr, R. Q.; Bell, A. T.; Theodorou, D. N. *J. Phys. Chem.* **1994**, *98*, 11948−11961.
(28) Goodbody, S. J.; Watanabe, K.; MacGowan, D.; Walton, J. P. R. B.; Quirke, N. *J. Chem. Soc., Faraday Trans.* **1991**, *87*, 1951−1958.
(29) Press, W. H.; Teukolsky, S. A.; Vetterling, W. T.; Flannery, B. P. *Numerical Recipes in Fortran. The Art of Scientific Computing*, 2nd ed.; Cambridge University Press: Cambridge, 1994.
(30) McQuarrie, D. A. *Statistical Mechanics*; Harper Collins: New York, 1976.
(31) Snurr, R. Q.; Bell, A. T.; Theodorou, D. N. *J. Phys. Chem.* **1993**, *97*, 13742−13752.
(32) Allen, M. P.; Tildesley, D. J. *Computer Simulation of Liquids*; Oxford University Press: New York, 1987.
(33) Olson, D. H.; Kokotailo, G. T.; Lawton, S. L.; Meier, W. M. *J. Phys. Chem.* **1981**, *85*, 2238−2243.
(34) Alberti, A.; Davoli, P.; Vezzalini, G. *Z. Kristallogr.* **1986**, *175*, 249−256.
(35) Pluth, J. J.; Smith, J. V. *Am. Mineral.* **1990**, *75*, 501−507.
(36) Lobo, R. F.; Davis, M. E. *J. Am. Chem. Soc.* **1995**, *117*, 3766−3779.
(37) Lobo, R. F.; Pan, M.; Chan, I.; Medrud, R. C.; Zones, S. I.; Crozier, P. A.; Davis, M. E. *J. Phys. Chem.* **1994**, *98*, 12040−12052.
(38) Adair, B.; Chen, C. Y.; Wan, K. T.; Davis, M. E. *Microporous Mater.* **1996**, *7*, 261−270.
(39) Corma, A.; Davis, M.; Fornes, V.; Gonzalez-Alfaro, V.; Lobo, R.; Orchilles, A. V. *J. Catal.* **1997**, *167*, 438−446.
(40) Keffer, D.; Davis, H. T.; McCormick, A. V. *Adsorption* **1996**, *2*, 9−21.
(41) Deem, M. W.; Newsam, J. M.; Creighton, J. A. *J. Am. Chem. Soc.* **1992**, *114*, 7198−7207.
(42) Kärger, J.; Ruthven, D. M. *Diffusion in Zeolites*; Wiley: New York, 1992.
(43) Macedonia, M.; Maginn, E. J.; Bicerano, J.; Garcés, J. Presented at the AIChE Annual Meeting, Los Angeles, CA, 1997.
(44) Snurr, R. Q.; June, R. L.; Bell, A. T.; Theodorou, D. N. *Mol. Simul.* **1991**, *8*, 73−92.
(45) Beenakker, J. J. M.; Borman, V. D.; Krylov, S. Y. *Chem. Phys. Lett.* **1995**, *232*, 379−382.